Polyoxometalates RESEARCH ARTICLE

A high-nuclearity vanadium(III,IV) cyclic coordination cluster with small ground spin state

Wei-Peng Chen, [1, 2] Yuan-Qi Zhai,[1] Qian-Cheng Luo,[1] Xia-Li Ding,[3] Anatoly R. Melnikov,[4] Sergey L. Veber,[4] Petr Neugebauer,[5] Joris van Slageren, [6] Yingqiu Dai, [7] Ji-Hu Su, [7] Xing Rong, [7] Zhenxing Wang, [8] Zhongwen Ouyang, [8] Ismael Francisco Diaz-Ortega, [9] Hiroyuki Nojiri [10] and Yan-Zhen Zheng [1]

[1] *Frontier science and technology, State Key Laboratory of Electrical Insulation and Power Equipment, Xi'an Key Laboratory of Electronic Devices and Material Chemistry, School of Chemistry, Xi'an Jiaotong University, Xi'an 710054, China*
[2] *School of Materials Science and Engineering, Shaanxi University of Technology, Hanzhong 723001, China*
[3] *Shaanxi Science and Technology Holding Institute, Xi'an 710016, China*
[4] *International Tomography Center of the Siberian Branch of the Russian Academy of Sciences, 3a, Institutskaya Str., Novosibirsk 630090, Russia*
[5] *Central European Institute of Technology, Brno University of Technology, Purkynova 123, 61200 Brno, Czech Republic*
[6] *Institut für Physikalische Chemie, Universität Stuttgart, Pfaffenwaldring 55, 70569 Stuttgart, Germany*
[7] *Hefei National Laboratory for Physical Sciences at the Microscale and Department of Modern Physics, CAS Key Laboratory of Microscale Magnetic Resonance, Synergetic Innovation Center of Quantum Information and Quantum Physics, University of Science and Technology of China, Hefei 230026, China*
[8] *Wuhan National High Magnetic Field Centre & School of Physics, Huazhong University of Science and Technology, Wuhan 430074, China*
[9] *Departamento de Químicay Física, Áreade Química Inorgánica-CIESOL, Universidad de Almería, Carretera Sacramento s/n, 04120 La Cañada de San Urbano (Almería), Spain*
[10] *Institute of Materials Research (IMR), Tohoku University, Katahira, Sendai 980-8577, Japan*

Received: 10 September 2026; **Revised:** 14 October 2026; **Accepted:** 19 October 2026

Address correspondence to Yuan-Qi Zhai, zhaiyuanqi@xjtu.edu.cn; Xia-Li Ding, dxl1457337646@163.com; Yan-Zhen Zheng, zheng.yanzhen@xjtu.edu.cn.

Cite This: *Polyoxometalates*, 2027, *6*, 9140171 Read Online

ABSTRACT: Low-valent vanadium(III) with d^2 electronic configuration, which can generate significant magnetic anisotropy, is highly desirable for the construction of high-performance molecule-based magnetic materials. Such lightweight and flexible magnetic materials cannot be realized by conventional inorganic or alloy-based permanent magnets. However, owing to the facile oxidation of vanadium(III), the synthesis of stable complexes containing highly reduced V(III) or mixed low-valent V(III,IV) centers remains extremely challenging. To date, only a limited number of V(III) or V(III,IV)-based coordination complexes or clusters have been isolated, most of which possess a nuclearity lower than eighteen. Herein, we report the self-assembly of a giant V(III,IV) cluster, namely $\{V^{III}_{20}V^{IV}_{2}O_8(OH)_8(CH_3COO)_{24}(CH_3CH_2O)_{20}\}\cdot 5CH_3CH_2OH$ (**V_{22}**), from a trinuclear vanadium precursor. The resulting large **V_{22}** cyclic coordination cluster exhibits an unusual small triplet ground spin state, which arises from antiferromagnetic exchange interactions. Moreover, this cluster system is detectable by electron paramagnetic resonance (EPR) spectroscopy and displays prominent quantum characteristics.

KEYWORDS: Low-valent, Vanadium(III), Coordination cluster, EPR spectroscopy, DFT calculations.

1 Instruction

Cluster-based materials represent a cutting-edge research hotspot, valued for their unique molecular architectures and considerable potential in magnetism, catalysis, and energy [1-8]. Upon the assembly of metal ions into cyclic frameworks, the aggregates exhibit distinctive properties such as electrical conductivity, biological activity, photosensitivity, and quantum oscillations [9-12]. However, targeted synthesis of cyclic coordination clusters (CCCs) remains challenging [13], and most known examples are serendipitous. Solvent evaporation affords cycles including $\{Cr_7M\}$ (M = Zn, Mn, Ni) [14], $\{Ni_{24}\}$ [15], $\{Fe_{28}\}$ [16], $\{Mn_{84}\}$ [17] and $\{Pd_{84}\}$ [18]. Anion-templated solvothermal synthesis yields lanthanide rings $\{Dy_{72}\}$ [19], $\{Gd_{140}\}$ [20], along with heterometallic analogues $\{Cr_8Ln_8\}$ [21] and $\{Ni_{36}Gd_{102}\}$ [22]. Molybdenum oxide cyclic clusters $\{Mo_{154}\}$ [23] and $\{Mo_{176}\}$ [24] form via pH-tuned condensation of inorganic oxoacids. Despite these advances, vanadium-based CCCs are rare [25], and low-valent V(III) analogues are especially scarce [26,27].

Vanadium-based chemistry is usually dominated by higher oxidation states, such as vanadium pentoxide and the extensive family of oxyanions including orthovanadate and vanadyl ions [28]. However, the V(V) cation possesses no electrons in the 3*d* orbitals and thus cannot serve as a source of magnetic moments

Just Accepted

for magnetic materials. There is considerable interest in studying the magnetic properties of low-valent V(III) species owing to their predicted large zero-field splitting parameters, a key factor for designing magnetic materials with strong anisotropy [26,27,29-40]. However, the synthesis of such low-valent V(III) complexes remains very challenging because V(III) is highly reductive and readily reacts with oxygen and other redox-active species [26].

To date, known vanadium complexes include "fully oxidized" V(V) [25], "mixed higher-valent" V(V,IV) [41-45], and "purely reduced" V(IV) [46-51], which represent the most commonly encountered oxidation states. Only a limited number of V(III) or V(III,IV) complexes have been reported; these species were synthesized from precursors including trivalent $[VCl_3]$ [52], $[VCl_3(thf)_3]$ [39,53-54], $[V(acac)_3]$ [40], $[V_3O(O_2CPh)_6(H_2O)_3]Cl$, $[V_3O(O_2CMe)_6(py)_3]ReO_4$ [27,53], and tetravalent $VOSO_4$ [55]. However, most of the reported complexes exhibit nuclearity lower than 18; examples include ring-like V(III) clusters such as $\{V^{III}_{10}\}$, $\{V^{III}_8\}$ [27], and species like $\{V^{III}_3V^{IV}_8\}$ [56], $\{V^{III}_{12}V^{IV}\}$ [53], $\{V^{III}_8V^{IV}_8\}$ [56], $\{V^{III}_{16}V^{IV}_2\}$ [54], among others.

Inspired by these pioneering works, we used a water-coordinated trinuclear precursor $[V_3O(H_2O)_3(CH_3COO)_6]Cl{\cdot}3.5H_2O$ as the starting material [57], and introduced reductive organic amines to convert high-valent vanadium ions into low-valent ones. Under solvothermal conditions, the preformed V(III) clusters dissociated, partially oxidized, and reassembled into a larger cluster, namely $\{V^{III}_{20}V^{IV}_2O_8(OH)_8(CH_3COO)_{24}(CH_3CH_2O)_{20}\}{\cdot}5CH_3CH_2OH$ (**V**$_{22}$), which has the record high nuclearity for V(III)-based clusters. Beyond its large nuclearity, **V**$_{22}$ is a CCC with an interesting boat-shaped architecture and a low-lying triplet ground spin state that can be probed by electron paramagnetic resonance (EPR) spectroscopy. The remarkable quantum behavior of **V**$_{22}$ stems from strong antiferromagnetic interactions among the vanadium sites, especially within the V(III)-V(III) pairs (*vide infra*).

2 Results and discussion

2.1 Crystal Structure and Solution Stability

Single crystal X-ray diffraction analysis shows that the CCC **V**$_{22}$ crystallizes in the orthorhombic space group *Pccn* (Table S1 in the ESM), and features a novel ring-like metal core containing twenty V(III) ions and two V(IV) ions. The polyhedral representation in Fig. 1 shows that the ring-shaped metal core of **V**$_{22}$ can be divided into two $\{V^{III}_2\}$, four $\{V^{III}_3\}$ and two $\{V^{III}_2V^{IV}\}$ fragments linked together by four μ-OH^-, six μ_3-O^{2-} and twenty μ-carboxylates. The $\{V^{III}_2\}$ units consist of two edge-sharing regular $\{VO_6\}$ octahedra bound by two μ-ethoxides and one μ-carboxylate, and two adjacent $\{V^{III}_2\}$ units are connected by two $\{V^{III}_3\}$ triangles through the μ-OH^- groups. The $\{V^{III}_3\}$ unit is further formed by three μ-ethoxide groups located in opposite direction to the central μ_3-OH^- group, thus holding together three edge-sharing regular $\{VO_6\}$ octahedra to form the truncated $\{V^{III}_3\}$ cubane. Each V(III) ion in the $\{V^{III}_3\}$ units is also linked to the neighboring $\{V^{III}_2V^{IV}\}$ and $\{V^{III}_3\}$ fragments. The two mixed-valent $\{V^{III}_2V^{IV}\}$ triangles consist of two $\{V^{III}O_6\}$ polyhedra and one trigonal-bipyramid $\{V^{IV}O_5\}$ polyhedron by edge-sharing via ethoxide group and one 2.11 (Harris notation [58]) acetate ligands. All the vanadyl centers has an averaged 1.60 Å V=O bond and other four V–O bonds ranging from 1.91 Å to 2.21 Å.

The cyclic-like cluster core can also be viewed as two distorted Anderson-type $\{V^{III}_6V^{IV}\}$ units [58-60], which are bridged by a pair of $\{V^{III}_4\}$ chains to form this macrocyclic architecture (Fig. S1 in the ESM). Three $\{V^{III}O_6\}$ octahedra share

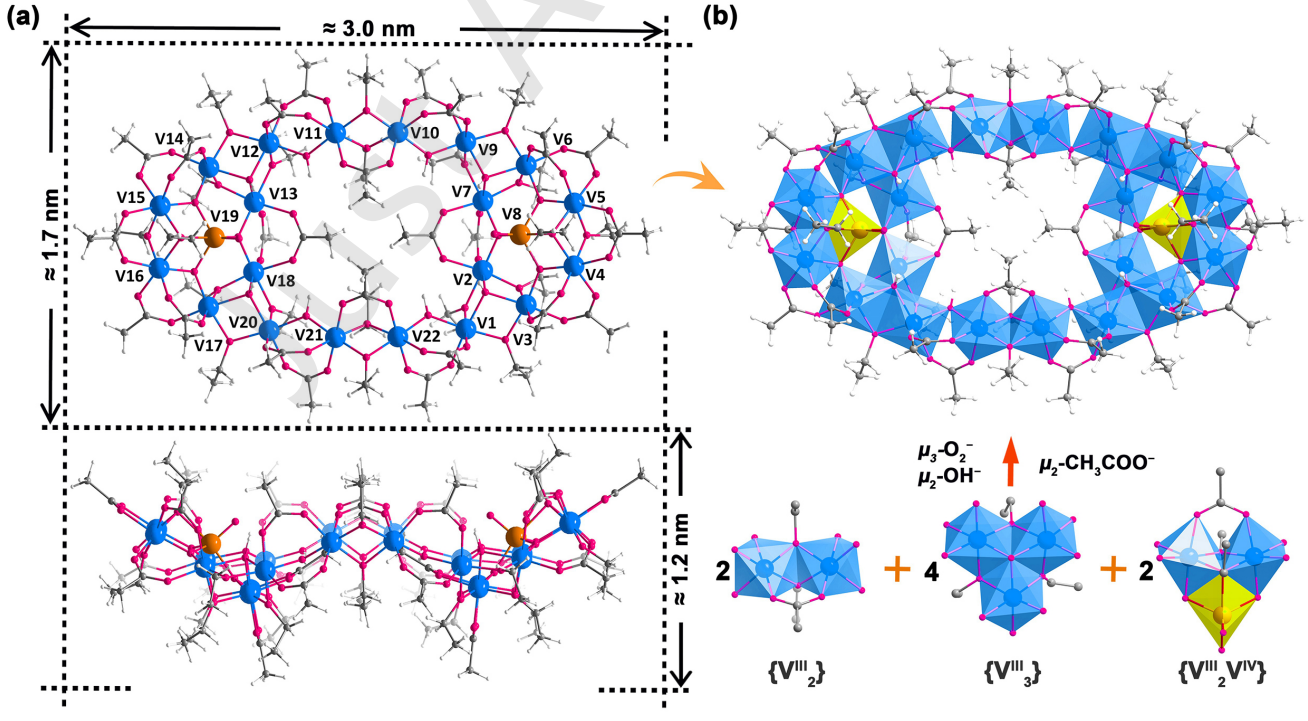

Figure 1 Molecular structure of **V**$_{22}$ in ball-and-stick (a) and polyhedron (b) styles. The cyclic-like core can be viewed as assembled from two $\{V^{III}_2\}$, four $\{V^{III}_3\}$ and two $\{V^{III}_2V^{IV}\}$ fragments. Color codes: V^{III}, blue; V^{IV}, yellow; O, red; C, gray; H, white.

an edge to generate $\{V^{III}_2\}$ dimeric units, which are further linked to a cyclic $\{V^{III}_6\}$ ring. At the center of this $\{V^{III}_6\}$ ring resides a

USTA Accepted

distorted $\{V^{IV}O_5\}$ polyhedron via edge-sharing with two adjacent $\{V^{III}_2\}$ units, thereby completing the distorted Anderson-type architecture. Importantly, the V–O–V angles and separations between V(III)···V(III) and V(III)···V(IV) range from 96.7° to 126.3°, 2.97 to 3.47 Å, and 3.05 to 3.41 Å (Fig. S2 in the ESM), respectively; all these values fall within ranges similar to those reported for other compounds [52-56]. The space-filling diagram of $\mathbf{V_{22}}$ reveals that the size of this molecule is *ca.* 3.0 nm in length and *ca.* 1.2 nm in thickness (Fig. S3 in the ESM).

The vanadium ions in $\mathbf{V_{22}}$ predominantly exhibit a formal +3 oxidation state, except for two tetravalent sites, labelled V8 and V19 (see Table S2 for bond valence sums). This finding is further corroborated by X-ray photoelectron spectroscopy (XPS) characterization of the $\mathbf{V_{22}}$ cluster (Fig. 2(a)). The deconvoluted XPS results reveal that the $\mathbf{V_{22}}$ cluster is dominated by V(III) species alongside a minor fraction of V(IV). The corresponding binding energies of V2$p_{3/2}$ and V2$p_{1/2}$ are 514.63 eV and 522.3 eV for V(III), and 516.34 eV and 524.46 eV for V(IV) (Fig. S4 and Table S3 in the ESM), consistent with literature precedents [62]. Moreover, the coordination modes of these vanadium centers are highly characteristic of their respective oxidation states because the V(III) centers favour regular octahedral $\{VO_6\}$ geometry, while V(IV) ions form highly distorted square-pyramidal $\{VO_5\}$.

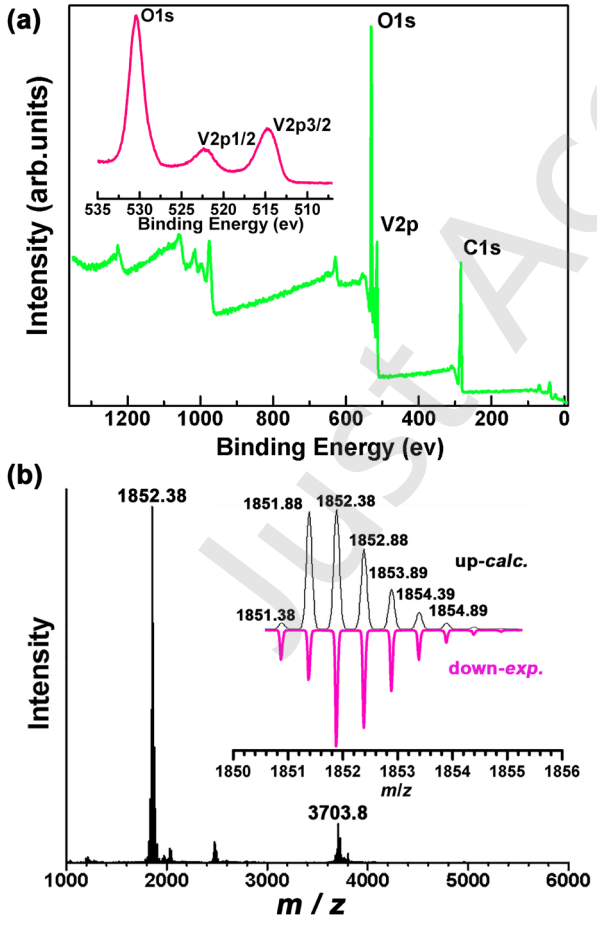

Figure 2 (a) The XPS spectrum of $\mathbf{V_{22}}$. The vanadium V2p energy window is shown inset; (b) Positive-mode ESI-MS spectrum of $\mathbf{V_{22}}$ in acetonitrile solution. Inset: ESI-MS spectra in the range from 1850 to 1855 (m/z). Pink: experimental peaks. Black: calculated peaks.

Under sonication, the solid $\mathbf{V_{22}}$ is sparingly soluble in CH_3CN, but insoluble in H_2O. Electrospray ionization mass spectrometry (ESI-MS) shows dominant peaks at *m/z* 1852.38 and 3703.8 (Fig. 2(b)), which correspond to the plausible molecular formulas of $\{H_2V_{22}O_8(OH)_8(CH_3COO)_{24}(CH_3CH_2O)_{20}\}^{2+}$ (*calcd. m/z* = 1852.52) and $\{HV_{22}O_8(OH)_8(CH_3COO)_{24}(CH_3CH_2O)_{20}\}^{+}$ (*calcd. m/z* = 3704.04), respectively. Notably, all peaks are in good agreement with the calculated isotope patterns (Figs. 2(b) and S5 in the ESM), implying that $\mathbf{V_{22}}$ maintains its structural integrity in CH_3CN.

2.2 Magnetic Properties

The room-temperature $\chi_m T$ product of the polycrystalline $\mathbf{V_{22}}$ sample was measured to be 16.4 $cm^3 \cdot K \cdot mol^{-1}$, which is lower than the theoretical value (20.75 $cm^3 \cdot K \cdot mol^{-1}$) for the sum of uncoupled 20 V(III) (S = 1) and 2 V(IV) (S = 1/2) ions, assuming g = 2 (as shown in Fig. 3(a)). Upon cooling, the $\chi_m T$ products steadily decreased to a minimum of 2.2 $cm^3 \cdot K \cdot mol^{-1}$ at 2 K, indicating substantial antiferromagnetic interactions. The molar susceptibility from 150 to 300 K was well-fitted by the Curie-Weiss equation with C = 30.6 $cm^3 \cdot K \cdot mol^{-1}$ and θ = –262.0 K (Fig. 3(a), inset). The large negative θ value suggests strong antiferromagnetic coupling among the vanadium ions. The isothermal field-dependent magnetization (M *vs.* H) at 2 K reaches 4.62 $N\mu_B$ at 7 T without saturation (Fig. 3(b)), also indicative of significant antiferromagnetic coupling within the cluster. Alternating current (ac) susceptibility measurements for $\mathbf{V_{22}}$ under zero dc field reveal no frequency-dependent susceptibility signals, indicating the absence of single-molecule magnet behavior down to 2 K (Fig. S6 in the ESM).

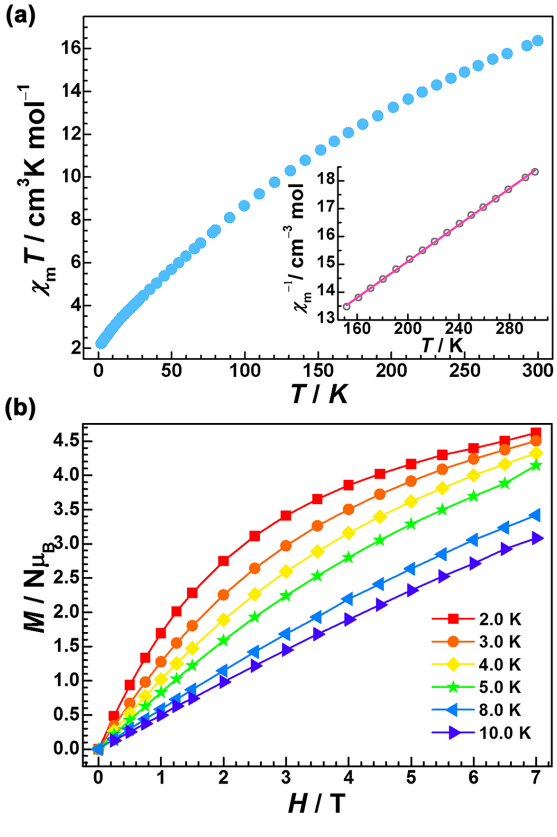

Figure 3 (a) The temperature-dependent molar susceptibility under 1000 Oe magnetic field and in the temperature range from 2 to 300 K. Inset: the plot of χ_m^{-1} *vs.* T; (b) The isothermal field-dependent magnetization at 2 – 10 K.

Just Accepted

2.3 Electronic Paramagnetic Resonance Spectra

The continuous wave (CW) electron paramagnetic resonance spectra of $\mathbf{V_{22}}$ polycrystalline powder were recorded in the standard first-derivative mode over the temperature range from 3.8 to 20 K, as shown in Fig. 4. The spectra are symmetric and composed of two-peak structure. The first peak was located in the vicinity of 350 mT, while the second one appears around 180 mT. Upon heating, the shape of the spectra remains consistent throughout the specified temperature range, with strong decay of the overall signal intensity already at ~20 K. Presumably, the observed temperature behavior can be attributed to the population, at higher temperatures, of the low-lying high-spin states within the $\mathbf{V_{22}}$ system. These states cause the X-band EPR signal to vanish due to the zero-field splitting present in the corresponding V(III) ions. The reliable detection of an X-band EPR signal at $T < 20$ K is consistent with the presence of V(IV) Kramers ions in $\mathbf{V_{22}}$ structure, and also demonstrates that they retain their paramagnetic character despite the very strong antiferromagnetic coupling that dominates in the $\mathbf{V_{22}}$ system (Fig. 3(a)). The observation of a "half-field" EPR line at 180 mT suggests that the paramagnetic species remaining at very low temperature form a triplet (or higher multiplicity) ground state.

Furthermore, the high-frequency/field electron paramagnetic resonance (HF-EPR) spectra of $\mathbf{V_{22}}$ powder were recorded at series of high frequencies (60-260 GHz and 300-380 GHz on two different spectrometers, see ESM) and low temperature (4.2 K), as depicted in Fig. S7 in the ESM. The curves show a broad first-differential spectrum with a large peak-to-peak width, and the simulation curves calculated with the best-fit parameters of g = 1.98. The temperature-dependent HF-EPR spectra were also measured (Fig. S7 in the ESM), the shapes of curves changed due to the temperature-dependent Boltzmann population of different spin states in the system.

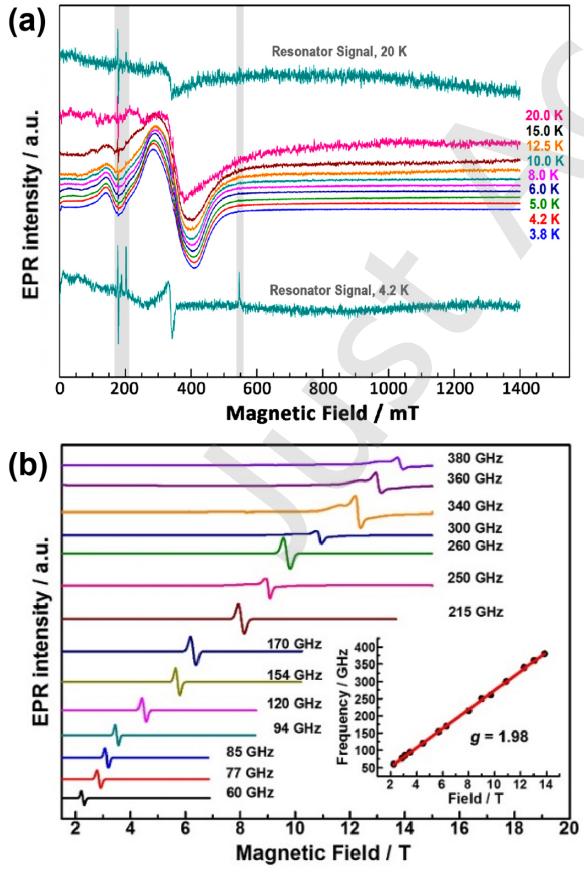

Figure 4 (a) Temperature-dependent X-band CW EPR of $\mathbf{V_{22}}$, where the grey-shaded areas represent regions containing the signals of the EPR resonator; (b) HF-EPR spectra of $\mathbf{V_{22}}$ recorded at 4.2 K under different frequencies (60 – 380 GHz). Inset: Microwave frequency versus resonance field for the most absorbed point observed.

2.4 *Ab initio* calculations on magnetic anisotropy

The individual magnetic anisotropies of the V(III) ions were investigated using the OPENMOLCAS package [62]. The mononuclear fragments of separated individual V(III) are used in the calculations, which are totally ten asymmetric V(III) ions in $\mathbf{V_{22}}$, as shown in Figs 5b and S8-S11 in the ESM.

The neighboring metal ions were replaced using the closed-shell Ga(III) and Ge(IV)-embedding *ab initio* model potential (AIMP) [63]. The electronic structures of mononuclear V(III) fragments were calculated via the complete active space self-

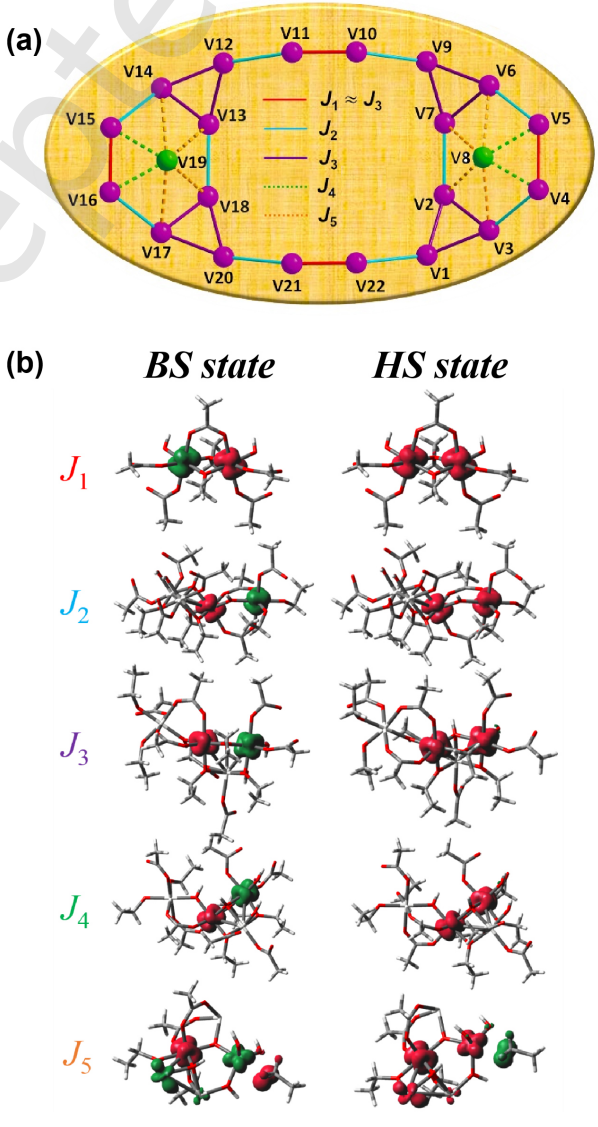

Figure 5. The magnetic coupling scheme of the metal centers in $\mathbf{V_{22}}$, with J_1 – J_5 defined according to the connection ways of the metal centers. The bottom shows broken-symmetry (BS) and high-spin (HS) density map of selected di-nuclear fragments from the whole $\mathbf{V_{22}}$ structure. The isovalue surface represented corresponds to a value of 0.01 e^-/bohr^3. The red regions indicate positive spin populations while green regions indicate negative ones.

Just Accepted

consistent field (CASSCF) approach [64]. Thus, the *g* tensors and zero field splitting (ZFS) tensors (*D*) for individual V(III) ions are obtained using SINGLE_ANISO program [65]. From Table S4 in the ESM we can see all the *g* (g_x, g_y, g_z) values are close to 1.99.

For V10 and V11, though ligand field excitation levels of triplets are not largely split (Table S5 in the ESM), the magnitude of *D* values were determined to be around –0.95 cm^{-1}. For V1, V2, V3, V6, V7 and V9 of which sites are locating in two {V_3} triangles an enhanced easy axis *D* value of –1.32 cm^{-1} in average is found. For the rest two metal sites (V4 and V5), the *D* = –0.89 cm^{-1} are derived, which is even smaller than V10 and V11. Together with the exchange coupling results from broken-symmetry calculations (see below), the magnetic anisotropies of the V(III) ions are negligible compared with exchange coupling of V(III)-V(III) and V(III)-V(IV).

2.5 Broken-symmetry calculations on exchange couplings

The exchange coupling constants (*J*) were computed using the broken-symmetry method, concentrating on selected di-nuclear fragments from the overall $\mathbf{V_{22}}$ structure while excluding other atoms to optimize computational efficiency, as depicted in Fig. 5. Based on the calculated *J* values provided in Table 1, we conclude that the DFT approach employing the B3LYP functional yields results indicative of solely antiferromagnetic interactions among various configurations of V(III)-V(III) and V(III)-V(IV).

The variations observed in the *J* values for V(III)-V(III) interactions can be ascribed to the presence of different bridging types, as previously detailed. Specifically, the shorter bond distances of 2.97 Å associated with bridging types I and III result in significantly pronounced antiferromagnetic interactions ($J_1 = J_3$ = –27.9 cm^{-1}) when compared to the longer distance of 3.38 Å found in type II (J_2 = –14.9 cm^{-1}). Regarding the interactions between V(III) and V(IV), although *J* values demonstrate significantly weaker magnitudes, they are primarily characterized by antiferromagnetic contributions. As such, the ground state could be viewed as two distant V(IV) ions (spin-1/2) ferromagnetic coupled via a bridge formed by twenty antiferromagnetic coupled V(III) ions, leading to an unusual small triplet ground spin state as observed by EPR spectra.

Table 1 Exchange coupling constants (*J*) for the five types of exchange pathways in the $\mathbf{V_{22}}$ system.

	Bridging ligands	Distance*	Magnitude
J_1	2 μ-ethoxides, 1 μ-carboxylate	2.97 Å	–27.9 cm^{-1}
J_2	1 μ-ethoxide, 2 μ-carboxylates	3.38 Å	–14.9 cm^{-1}
J_3	1 μ-ethoxide, 1 μ-OH^-	2.97 Å	–27.9 cm^{-1}
J_4	1 μ-ethoxide, 1 μ-OH^-	3.05 Å	–3.7 cm^{-1}
J_5	1 μ-OH^-	3.41 Å	–1.7 cm^{-1}

* The V-V distances presented here are averaged; for further details, please refer to Table S6 in the ESM.

At low temperature, the magnetic behavior is dominated by the strong V(III)–V(III) exchange pathways J_1 - J_3, which have the largest antiferromagnetic magnitudes and correspond to the shortest V···V distance. These pathways generate a strongly antiferromagnetic V(III) network and are mainly responsible for the pronounced decrease of $\chi_m T$, the large negative Weiss constant, and the unsaturated magnetization. In contrast, the V(III)–V(IV) couplings J_4 and J_5 are much weaker, and primarily determine the low-lying spin-state structure and the residual triplet ground state rather than the overall susceptibility.

3 Conclusions

To summarize, the largest mixed-valent vanadium (III, IV) cluster featuring a cyclic-like structure has been isolated through a precursor-based alcohol-thermal reaction. Magnetic measurement, along with EPR spectra, *ab initio* and DFT calculations, reveal strong antiferromagnetic exchange coupling within the V(III)-V(III) pairs, while the couplings involving V(III)-V(IV) are much weaker. Such a competing scenario finally results in an unusual small triplet ground spin state. Therefore, we believe this cluster-based vanadium(III,IV) material could be further used as a source of low-valent vanadium and potential quantum objects.

Electronic Supplementary Material: Supplementary material (Experiment section, synthesis schematic, crystal structural figures, ESI-MS spectra, HF-EPR spectra, supporting tables) is available in the online version of this article at https://doi.org/10.26599/POM.2026.9140171.

Data availability

All data needed to support the conclusions in the paper are presented in the manuscript and the Electronic Supplementary Material. Additional data related to this paper may be requested from the corresponding author upon request.

Acknowledgements

This work was financially supported by the National Natural Science Foundation of China (Nos. 22375157 and No. 22505194), Shaanxi Provincial Special Support Plan for Young Top-notch Talents, Shaanxi Provincial Natural Science Foundation (No. 2026JC-YBMS-0118), the Medical-Engineering Cross Project of the First Affiliated Hospital of XJTU (No. QYJC02), the Fundamental Research Funds for the Central Universities (No. xtr072024042), the Open Research Project of the Provincial Key Laboratory of Shaanxi University of Technology (No. SLGKFKT202633), the Talent Start-up Fund from Shaanxi University of Technology (No. SLGRCQD052), the GIMRT Program of the Institute for Materials Research (Tohoku University, Sendai, Japan, No. 202405-RDKGE-0523) and the Special Research Fund for Industrial Innovation of Xi'an Jiaotong University-Shaanxi Non-ferrous Metals Holding Group Co., Ltd Research Institute. Dr. X.-L. Ding thanks Shaanxi Qinchuangyuan "Scientists + Engineers" Team Project (No. 2025QCY-KXJ-008). Dr. S. L. Veber and Dr. A. R. Melnikov thank the Ministry of Science and Higher Education of the RF for granting access to EPR equipment. Dr. P. Neugebauer and Prof. J. van Slageren thank the German Research Foundation (DFG) for funding (SPP1601, INST41/863).

Declaration of competing interest

The authors have no competing interests to declare that are relevant to the content of this article.

Just Accepted

Author contribution statement

W.-P. C., Y.-Q. Z., Q.-C. L., and X.-L. D.: Data curation, validation, writing the manuscript, experimental design, funding acquisition. A. R. M., S. L. V., P. N., J. v. S., Y. D., J.-H. S., X. R., Z. W., Z. O., I. F. D., and H. N.: Data collection and data curation. Y.-Z. Z.: Project administration, revising the manuscript, funding acquisition. All the authors have approved the final manuscript.

Use of AI statement

None.

References

[1] Xu, Q.-F.; Wu, R.-T.; Long, L.-S.; Zheng, L.-S. Ultralow-temperature magnetic refrigeration inorganic materials: from designed synthesis to adiabatic demagnetization refrigeration. *Acc. Chem. Res.* **2025**, *58*, 2898-2909.

[2] Xu, N.; Chen, W.-M.; Ding, Y.-S.; Zheng, Z.-P. A cubic tinkertoy-like heterometallic cluster with a record magnetocaloric effect. *J. Am. Chem. Soc.* **2024**, *146*, 9506-9511.

[3] Chen, J.-N.; Zhang, S.; Hu, S.-X.; Wang, C.; Long, L.-S.; Zheng, L.-S.; Kong, X.-J. Homocentric chirality and magnetism enable strong NIR magneto-optical activity in a chiral DyFe3 cluster. *J. Am. Chem. Soc.* **2026**, *148*, 9851-9859.

[4] Yu, F.-Y.; Lang, Z.-L.; Wang, X.; Sun, J.; Liu, Y.-C.; Tan, H.-Q.; Ge, J.-J.; Li, Y.-G.; Kang, Z.-H. Synergistic enhancement of Pt electrocatalyst stability and activity in hydrogen oxidation reaction by polyoxometalate and carbon dot co-boosting. *Sci. Bull.* **2025**, *70*, 3154-3163.

[5] Zhang, B.-T.; Qiu, T.-Y.; Li, Y.-Q.; Li, Y.; Yu, F.-Y.; Dong, H.-L.; Wang, Y.-H.; Li, Y.-G.; Tan, H.-Q. Well-dispersed manganese-oxo clusters as anode materials for high-performance lithium ion batteries. *Nano Lett.* **2024**, *24*, 11512-11519.

[6] Lv, J.-Q.; Lang, Z.-L.; Fu, J.-Q.; Lan, Q.; Liu, R.; Zang, H.-Y.; Li, Y.-G.; Ye, D.-D.; Streb, C. Molecular iron oxide clusters boost the oxygen reduction reaction of platinum electrocatalysts at near-neutral pH. *Angew. Chem. Int. Ed.* **2022**, *61*, e202202650.

[7] Hu, B.; Liu, B.; Pan, Q.; Ren, H.; Yu, F.; Du, Q.; Li, Y.; Zang, H.-Y. Structural effects in polyoxometalate-based supramolecular assemblies for enhanced proton conduction. *Angew. Chem. Int. Ed.* **2026**, *65*, e17958.

[8] Chen, Y.-Z.; Cui, Y.-Z.; Zhang, Y.; Zhong, R.-L.; Liu, Q.; Li, J.; Su, Z.-M.; Zang, H.-Y. Rational design of a {$InCu_6$} heterometallic oxo cluster for superior proton conduction: mechanistic insights and humidity gradient-based power generation. *Angew. Chem. Int. Ed.* **2026**, *65*, e6584076.

[9] Baniodeh, A.; Liang, Y.; Anson, C. E.; Magnani, N.; Powell, A. K.; Unterreiner, A. N.; Seyfferle, S.; Slota, M.; Dressel, M.; Bogani, L.; Goß, K. Unraveling the influence of lanthanide ions on intra- and inter-molecular electronic processes in $Fe_{10}Ln_{10}$ nano-toruses. *Adv. Funct. Mater.* **2014**, 24, 6280-6290.

[10] Guedes, G.; Wang, S.; Fontana, F.; Figueiredo, P.; Lindén, J.; Correia, A.; Pinto, R. J. B.; Hietala, S.; Sousa, F. L.; Santos, H. A. Dual-crosslinked dynamic hydrogel incorporating {Mo_{154}} with pH and NIR responsiveness for chemo-photothermal therapy. *Adv. Mater.* **2021**, *55*, 2007761.

[11] Shi, D.; Yang, X.; Chen, H.; Jiang, D.; Liu, J.; Ma, Y.; Schipper, D.; Jones, R. A. Large Ln_{42} coordination nanorings: NIR luminescence sensing of metal ions and nitro explosives. *Chem. Commun.* **2019**, *55*, 13116-13119.

[12] Carretta, S.; Santini, P.; Amoretti, G.; Guidi, T.; Copley, J. R. D.; Qiu, Y.; Caciuffo, R.; Timco, G.; Winpenny, R. E. P. Quantum oscillations of the total spin in a heterometallic antiferromagnetic ring: Evidence from neutron spectroscopy. *Phys. Rev. Lett.* **2007**, *98*, 167401.

[13] Timco, G. A.; Faust, T. B.; Tuna, F.; Winpenny, R. E. P. Linking heterometallic rings for quantum information processing and amusement. *Chem. Soc. Rev.* **2011**, *40*, 3067-3075.

[14] Garlatti, E.; Albring, M. A.; Baker, M. L.; Docherty, R. J.; Mutka, H.; Guidi, T.; Sakai, V. G.; Whitehead, G. F. S.; Pritchard, R. G.; Timco, G. A.; Tuna, F.; Amoretti, G.; Carretta, S.; Santini, P.; Lorusso, G.; Affronte, M.; McInnes, E. J. L.; Collison, D.; Winpenny, R. E. P. A detailed study of the magnetism of chiral {Cr_7M} rings: an investigation into parametrization and transferability of parameters. *J. Am. Chem. Soc.* **2014**, *136*, 9763-9772.

[15] Dearden, A. L.; Parsons, S.; Winpenny, R. E. P. Synthesis, structure, and preliminary magnetic studies of a Ni(24) wheel. *Angew. Chem. Int. Ed.* **2001**, *40*, 151-154.

[16] Zhang, Z. M.; Li, Y. G.; Yao, S.; Wang, E. B.; Wang, Y. H.; Clérac, R. Enantiomerically pure chiral {Fe_{28}} wheels. *Angew. Chem. Int. Ed.* **2009**, *48*, 1581-1584.

[17] Tasiopoulos, A. J.; Vinslava, A.; Wernsdorfer, W.; Abboud, K. A.; Christou, G. Giant single-molecule magnets: a {Mn_{84}} torus and its supramolecular nanotubes. *Angew. Chem. Int. Ed.* **2004**, *43*, 2117-2121.

[18] Scullion, R. A.; Surman, A. J.; Xu, F.; Mathieson, J. S.; Long, D.-L.; Haso, F.; Liu, T.; Cronin, L. Exploring the symmetry, structure, and self-assembly mechanism of a gigantic seven-fold symmetric {Pd_{84}} wheel. *Angew. Chem. Int. Ed.* **2014**, *53*, 10032-10037.

[19] Qin, L.; Yu, Y.-Z.; Liao, P.-Q.; Xue, W.; Zheng, Z. P.; Chen, X.-M.; Zheng, Y.-Z. A "molecular water pipe": a giant tubular cluster {Dy_{72}} exhibits fast proton transport and slow magnetic relaxation. *Adv. Mater.* **2016**, *28*, 10772-10779.

[20] Zheng, X.-Y.; Jiang, Y.-H.; Zhuang, G.-L.; Liu, D.-P.; Liao, H.-G.; Kong, X.-J.; Long, L.-S.; Zheng, L.-S. A gigantic molecular wheel of {Gd_{140}}: a new member of the molecular wheel family. *J. Am. Chem. Soc.* **2017**, *139*, 18178-18181.

[21] Qin, L.; Singleton, J.; Chen, W.-P.; Nojiri, H.; Engelhardt, L.; Winpenny, R. E. P.; Zheng, Y.-Z. Quantum Monte Carlo simulations and high-field magnetization studies of antiferromagnetic interactions in a giant hetero-spin ring. *Angew. Chem. Int. Ed.* **2017**, *56*, 16571-16574.

[22] Chen, W.-P.; Liao, P.-Q.; Jin, P.-B.; Zhang, L.; Ling, B.-K.; Wang, S.-C.; Chan, Y.-T.; Chen, X.-M.; Zheng, Y.-Z. The gigantic {$Ni_{36}Gd_{102}$} hexagon: a sulfate-templated "star-of-david" for photocatalytic CO_2 reduction and magnetic cooling. *J. Am. Chem. Soc.* **2020**, *142*, 4663-4670.

[23] Liu, T.; Diemann, E.; Li, H.; Dress, A. W. M.; Müller, A. Self-assembly in aqueous solution of wheel-shaped Mo_{154} oxide clusters into vesicles. *Nature* **2003**, *426*, 59-62.

[24] Imai, H.; Akutagawa, T.; Kudo, F.; Ito, M.; Toyoda, K.; Noro, S.-i.; Cronin, L.; Nakamura, T. Structure, magnetism, and ionic conductivity of the gigantic {Mo_{176}}-wheel assembly: $Na_{15}Fe_3Co_{16}[Mo_{176}O_{528}H_3(H_2O)_{80}]Cl_{27}{\cdot}450H_2O$. *J. Am. Chem. Soc.* **2009**, *131*, 13578-13579.

[25] Monakhov, K. Y.; Bensch, W.; Kögerler, P. Semimetal-functionalised polyoxovanadates. *Chem. Soc. Rev.* **2015**, *44*, 8443-8483.

[26] Dinda, R.; Garribba, E.; Sanna, D.; Crans, D. C.; Costa Pessoa, J. Hydrolysis, ligand exchange, and redox properties of vanadium compounds: implications of solution transformation on biological, therapeutic, and environmental applications. *Chem. Rev.* **2025**, *125*, 1468-1603.

[27] Laye, R. H.; Murrie, M.; Ochsenbein, S.; Bell, A. R.; Teat, S. J.; Raftery, J.; McInnes, E. J. Solvothermal syntheses of high-nuclearity vanadium (III) clusters. *Chem. Eur. J.* **2003**, *9*, 6215-6220.

[28] Sutradhar, M.; Da Silva, J. A. L.; Pombeiro, A. J. L. Introduction: Vanadium, Its Compounds and Applications. In *Vanadium Catalysis*, The Royal Society of Chemistry. **2020**, ch. 1, pp. 1-11.

[29] Atzori, M.; Morra, E.; Tesi, L.; Albino, A.; Chiesa, M.; Sorace, L.; Sessoli, R. Quantum coherence times enhancement in vanadium(IV)-based potential molecular qubits: the key role of the vanadyl moiety. *J. Am. Chem. Soc.* **2016**, *138*, 11234-11244.

[30] Xu, Q. F.; Liu, X. Y.; Wu, R. T.; Fu, M. Y.; Chen, M. T.; Xiang, J.-S.; Meng, Y.-S.; Liu, T.; Sun, P.-J.; Long, L.-S.; Zheng, L.-S. Temperature below 30 mK achieved by adiabatic demagnetization refrigeration. *J.*

Just Accepted

Am. Chem. Soc. **2025**, *147*, 27089-27094.

[31] Manvell, A. S.; Dunstan, M. A.; Gracia, D.; Hruby, J.; Kubus, M.; McPherson, J. N.; Palacios, E.; Weihe, H.; Hill, S.; Schnack, J.; Evangelisti, M.; Pedersen, K. S. A triangular frustrated Eu(II)-organic framework for sub-Kelvin magnetic refrigeration. *J. Am. Chem. Soc.* **2025**, *147*, 7597-7603.

[32] Tziotzi, T. G.; Gracia, D.; Dalgarno, S. J.; Schnack, J.; Evangelisti, M.; Brechin, E. K.; Milios, C. J. A $\{Gd_{12}Na_6\}$ molecular quadruple-wheel with a record magnetocaloric effect at low magnetic fields and temperatures. *J. Am. Chem. Soc.* **2023**, *145*, 7743-7747.

[33] Ferlay, S.; Mallah, T.; Ouahès, R.; Veillet, P.; Verdaguer, M. A room-temperature organometallic magnet based on Prussian blue. *Nature* **1995**, *378*, 701-703.

[34] Pedersen, K. S.; Perlepe, P.; Aubrey, M. L.; Woodruff, D. N.; Reyes-Lillo, S. E.; Reinholdt, A.; Voigt, L.; Li, Z.; Borup, K.; Rouzières, M.; Samohvalov, D.; Wilhelm, F.; Rogalev, A.; Neaton, J. B.; Long, J. R.; Clérac, R. Formation of the layered conductive magnet $CrCl_2(pyrazine)_2$ through redox-active coordination chemistry. *Nat. Chem.* **2018**, *10*, 1056-1061.

[35] Perlepe, P.; Oyarzabal, I.; Voigt, L.; Kubus, M.; Woodruff, D. N.; Reyes-Lillo, S. E.; Aubrey, M. L.; Negrier, P.; Rouzières, M.; Wilhelm, F.; Rogalev, A.; Neaton, J. B.; Long, J. R.; Mathonière, C.; Vignolle, B.; Pedersen, K. S.; Clérac, R. From an antiferromagnetic insulator to a strongly correlated metal in square-lattice $MCl_2(pyrazine)_2$ coordination solids. *Nat. Commun.* **2022**, *13*, 5766.

[36] Yang, Y.; Ji, J.; Feng, J.; Chen, S.; Bellaiche, L.; Xiang, H. Two-dimensional organic-inorganic room-temperature multiferroics. *J. Am. Chem. Soc.* **2022**, *144*, 14907-14914.

[37] Hatlevik, O.; Buschmann, W. E.; Zhang, J.; Manson, J. L.; Miller, J. S. Enhanced the magnetic ordering temperature and air stability of a mixed-valent vanadium hexacyanochromate(III) magnet to 99 °C (372 K). *Adv. Mater.* **1999**, *11*, 914-918.

[38] Khanra, S.; Kloth, M.; Mansaray, H.; Muryn, C. A.; Tuna, F.; Sañudo, E. C.; Helliwell, M.; McInnes, E. J. L.; Winpenny, R. E. P. Synthesis of molecular vanadium(III) phosphonates. *Angew. Chem. Int. Ed.* **2007**, *46*, 5568-5571.

[39] Tidmarsh, I. S.; Batchelor, L. J.; Scales, E.; Laye, R. H.; Sorace, L.; Caneschi, A.; Schnack, J.; McInnes, E. J. L. Tri-, tetra- and octa-metallic vanadium(III) clusters from new, simple starting materials: Interplay of exchange and anisotropy effects. *Dalton Trans.* **2009**, *43*, 9402-9409.

[40] Shaw, R.; Tuna, F.; Wernsdorfer, W.; Barra, A. L.; Collison, D.; McInnes, E. J. L. Large spin, magnetically anisotropic, octametallic vanadium(III) clusters with strong ferromagnetic coupling. *Chem. Commun.* **2007**, *48*, 5161-5163.

[41] Müller, A.; Krickemeyer, E.; Penk, M.; Walberg, H.-J; Bögge, H. Spherical mixed-valence $[V_{15}O_{36}]^{5-}$, an example from an unusual cluster family. *Angew. Chem. Int. Ed.* **1987**, *26*, 1045-1046.

[42] Müller, A.; Penk, M.; Rohlfing, R.; Krickemeyer, E.; Döring, J. Topologically interesting cages for negative ions with extremely high "coordination number": an unusual property of V-O clusters. *Angew. Chem. Int. Ed.* **1990**, *29*, 926-927.

[43] Chen, Q.; Goshorn, D. P.; Scholes, C. P.; Tan, X. L.; Zubieta, J. Coordination compounds of polyoxovanadates with a hexametalate core. chemical and structural characterization of $[V^{V}_6O_{13}[(OCH_2)_3CR]_2]^{2-}$, $[V^{V}_6O_{11}(OH)_2[(OCH_2)_3CR]_2]$, $[V^{IV}_4V^{V}_2O_9(OH)_4[(OCH_2)_3CR]_2]^{2-}$, and $[V^{IV}_6O_7(OH)_6](OCH_2)_3CR]_2]^{2-}$. *J. Am. Chem. Soc.* **1992**, *114*, 4667-4681.

[44] Monakhov, K. Y.; Linnenberg, O.; Kozłowski, P.; van Leusen, J.; Besson, C.; Secker, T.; Ellern, A.; López, X.; Poblet, J. M.; Kögerler, P. Supramolecular recognition influences magnetism in $[X@HV^{IV}_8V^{V}_{14}O_{54}]^{6-}$ self-assemblies with symmetry-breaking guest anions. *Chem. Eur. J.* **2015**, *21*, 2387-2397.

[45] Gumerova, N. I.; Rompel, A. Synthesis, structures and applications of electron-rich polyoxometalates. *Nat. Rev. Chem.* **2018**, *2*, 0112.

[46] Johnson, G. K.; Schlemper, E. O. Existence and structure of the molecular ion 18-vanadate(IV). *J. Am. Chem. Soc.* **1978**, *100*, 3645-3646.

[47] Tripathi, A.; Hughbanks, T.; Clearfield, A. The first framework solid composed of vanadosilicate clusters. *J. Am. Chem. Soc.* **2003**, *125*, 10528-10529.

[48] Zheng, S. T.; Zhang, J.; Li, B.; Yang, G. Y. The first solid composed of $\{As_4V_{16}O_{42}(H_2O)\}$ clusters. *Dalton Trans.* **2008**, *41*, 5584-5587.

[49] Hoshino, N.; Nakano, M.; Nojiri, H.; Wernsdorfer, W.; Oshio, H. Templating odd numbered magnetic rings: oxovanadium heptagons sandwiched by *β*-cyclodextrins. *J. Am. Chem. Soc.* **2009**, *131*, 15100-15101.

[50] Hegetschweiler, K.; Morgenstern, B.; Zubieta, J.; Hagrman, P. J.; Lima, N.; Sessoli, R.; Totti, F. Strong Ferromagnetic Interactions in $[V_8O_{14}(H_2taci)_2]$: An unprecedented large spin ground state for a vanadyl cluster. *Angew. Chem. Int. Ed.* **2004**, *43*, 3436-3439.

[51] Yamabayashi, T.; Atzori, M.; Tesi, L.; Cosquer, G.; Santanni, F.; Boulon, M.-E.; Morra, E.; Benci, S.; Torre, R.; Chiesa, M.; Sorace, L.; Sessoli, R.; Yamashita, M. Scaling up Electronic spin qubits into a three-dimensional metal-organic framework. *J. Am. Chem. Soc.* **2018**, *140*, 12090-12101.

[52] Laye, R. H.; Wei, Q.; Mason, P. V.; Shanmugam, M.; Teat, S. J.; Brechin, E. K.; Collison, D.; McInnes, E. J. L. A highly reduced vanadium (III/IV) polyoxovanadate comprising an octavanadyl square-prism surrounding a dimetallic vanadium(III) fragment. *J. Am. Chem. Soc.* **2006**, *128*, 9020-9021.

[53] Khanra, S.; Shaw, R.; Helliwell, M.; Tuna, F.; Muryn, C. A.; McInnes, E. J. L.; Winpenny, R. E. P. Families of molecular hexa- and trideca-metallic vanadium(III) phosphonates. *Materials* **2010**, *3*, 232-240.

[54] Tidmarsh, I. S.; Laye, R. H.; Brearley, P. R.; Shanmugam, M.; Sañudo, E. C.; Sorace, L.; Caneschi, A.; McInnes, E. J. A high-nuclearity, beyond "fully reduced" polyoxo(alkoxo)vanadium(III/IV) cage. *Chem. Commun.* **2006**, *24*, 2560-2562.

[55] Cao, J. P.; Xue, Y. S.; Hu, Z. B.; Luo, X. M.; Cui, C. H.; Song, Y.; Xu, Y. Exploring the magnetic interaction of asymmetric structures based on chiral V^{III}_8 clusters. *Inorg. Chem.* **2019**, *58*, 2645-2651.

[56] Tidmarsh, I. S.; Laye, R. H.; Brearley, P. R.; Shanmugam, M.; Sañudo, E. C.; Sorace, L.; Caneschi, A.; McInnes, E. J. L. Highly reduced, polyoxo(alkoxo)vanadium(III/IV) clusters. *Chem. Eur. J.* **2007**, *13*, 6329-6338.

[57] Fry, F. H.; Dougan, B. A.; McCann, N.; Ziegler, C. J.; Brasch, N. E. Characterization of novel vanadium(III)/acetate clusters formed in aqueous solution. *Inorg. Chem.* **2005**, *44*, 5197-5199.

[58] Coxall, R. A.; Harris, S. G.; Henderson, D. K.; Parsons, S.; Tasker, P. A.; Winpenny, R. E. Inter-ligand reactions: in situ formation of new polydentate ligands. *J. Chem. Soc. Dalton. Trans.* **2000**, 14, 2349-2356.

[59] Sharples, J. W.; Zheng, Y. Z.; Tuna, F.; McInnes, E. J. L.; Collison, D. Lanthanide discs chill well and relax slowly. *Chem. Commun.* **2011**, *47*, 7650-7652.

[60] Yvon, C.; Surman, A. J.; Hutin, M.; Alex, J.; Smith, B. O.; Long, D. L.; Cronin, L. Polyoxometalate clusters integrated into peptide chains and as inorganic amino acids: solution-and solid-phase approaches. *Angew. Chem. Int. Ed.* **2014**, *53*, 3336-3341.

[61] Mikuriya, M.; Kotera, T.; Adachi, F.; Bandow, S. A tetranuclear vanadium(III, III, IV, IV) complex formed by a reaction of bis (acetylacetonato)oxovanadium (IV) with a thiolate ligand. *Chem. Lett.* **1993**, *22*, 945-948.

[62] Fdez. Galván, I.; Vacher, M.; Alavi, A.; Angeli, C.; Aquilante, F.; Autschbach, J.; Lindh, R. OpenMolcas: from source code to insight. *J. Chem. Theory Comput.* **2019**, *15*, 5925-5964.

[63] López-Moraza, S.; Pascual, J. L.; Barandiarán, Z. Ab initio model potential embedded-cluster study of V^{2+} doped fluoroperovskites: effects of different hosts on the local distortion and electronic structure of $^4T_{2g}$-$^4A_{2g}$ laser levels. *J. Chem. Phys.* **1995**, *103*, 2117-2125.

[64] Pierloot, K. The $CASPT_2$ method in inorganic electronic spectroscopy: from ionic transition metal to covalent actinide complexes. *Mol. Phys.* **2003**, *101*, 2083-2094.

[65] Ungur, L.; Chibotaru, L. F. Ab initio crystal field for lanthanides. *Chem. Eur. J.* **2017**, *23*, 3708-3718.

Just Accepted

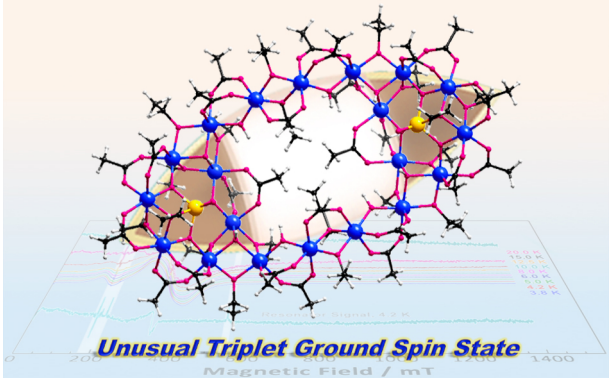

A high-nuclearity $\mathbf{V_{22}}$ cyclic coordination cluster containing mixed-valent V(III)/V(IV) centers has been synthesized, exhibiting an intriguing small ground spin state.

Just Accepted